Polymer 50 (2009) 2393–2401

Contents lists available at ScienceDirect

Polymer

journal homepage: www.elsevier.com/locate/polymer

Isothermal titration calorimetry, transmission electron microscopy, and field emission scanning electron microscopy of a main-chain viologen polymer containing bromide as counterions

Pradip K. Bhowmik [a,*], Marcos A. Cheney [b], Robin Jose [c], Haesook Han [a], Arghya Banerjee [d], Longzhou Ma [e], Lee D. Hansen [f]

[a] Department of Chemistry, University of Nevada Las Vegas, 4505 Maryland Parkway, Box 454003, Las Vegas, NV 89154, USA
[b] Department of Natural Sciences, University of Maryland Eastern Shores, Carver Hall, Room 1103, Princess Ann, MD 21853, USA
[c] Department of Chemistry, Rocky Mountain College, 1511 Poly Drive, Billings, MT 59102, USA
[d] Department of Aerospace Engineering Sciences, University of Colorado, 429 UCB, Boulder, CO 80309, USA
[e] Harry Center for Environmental Studies, University of Nevada Las Vegas 4505 Maryland Parkway, Box454009, Las Vegas, Box 454009, NV 89154, USA
[f] Department of Chemistry and Biochemistry, Brigham Young University, Provo, UT 84602, USA

ARTICLE INFO

Article history:
Received 28 December 2008
Received in revised form
15 March 2009
Accepted 18 March 2009
Available online 7 April 2009

Keywords:
Isothermal titration calorimetry
Transmission electron microscopy
Field emission scanning electron microscopy

ABSTRACT

The interaction of a main-chain viologen polymer containing bromide as counterions with water and aqueous potassium bromide over a broad range of concentrations was studied with isothermal titration calorimetry. The dilution process of this polymer was endothermic as opposed to flexible poly(sodium acrylate) and poly(sodium styrenesulfonate). This result may be related to the different mechanism of hydration of pyridinium and bromide groups in the main chain. It also exhibited aggregation phenomenon in both water and aqueous potassium bromide solutions as detected by transmission electron microscopy like other flexible and rigid-rod polyelectrolytes. As the polymer concentrations in aqueous solutions increase, the aggregated polymer exhibited more defined ordered structures than random structures observed at low polymer concentrations. Field emission scanning electron microscopy also revealed the effect of variation of concentration of aqueous potassium bromide on the morphology of the polymer matrix. At increasing concentrations of aqueous potassium bromide, the polymer structures became more ordered than those in low concentrations.

1. Introduction

Polyelectrolytes are an important class of macromolecules that contain dissociable ionic groups. When introduced into polar solvent, usually the universal solvent water, dissociation takes place so that electrically charged macromolecule is suspended in solution. The electrostatic interaction is operative between ionized groups inside the macromolecule, between the macromolecules, between the counterions, and between the macromolecule and counterion. Since this interaction is characterized by its long-range nature, the solution exhibits various interesting properties including the polyelectrolyte behavior very different from solutions of neutral polymers [1–6]. Recently, they have received resurrecting interest both for the construction of ordered solid-state structures from the interactions of various surfactants with the oppositely charged macromolecules and for the construction of functional multilayer assemblies by sequential layer-by-layer deposition technique through electrostatic interactions. These ordered structures offer a host of interesting properties ranging from improved mechanical property to optical, electrical, and even biological properties [7,8]. However, in contrast to the well understanding of the structures and dynamics of neutral polymers, there is undoubtedly a lack of clear molecular interpretations for many of the fundamental properties of charged polymers. On one hand, the different theoretical treatments that are usually used to understand their various aspects include the concept of an electrostatic persistent length, counterion condensation, descriptions of entangled solution behavior, couple-mode theory, electrolytic dissipation, and phase transitions in their solutions. On the other hand, the various experimental techniques that are commonly used to decipher structures and dynamics (i.e., intrachain and interchange interactions) of this class of polymers include static and dynamic light scattering, neutron spin echo, electrical conductivity, solution viscosity, viscoelasticity, nuclear magnetic and electron spin resonance spectroscopy [1–6,9,10]. The typical cationic polyelectrolytes

* Corresponding author. Tel.: +1 702 895 0885; fax: +1 702 895 4072.
E-mail address: pradip.bhowmik@unlv.edu (P.K. Bhowmik).

0032-3861/$ – see front matter © 2009 Elsevier Ltd. All rights reserved.
doi:10.1016/j.polymer.2009.03.046

that are used in various studies include poly(4-vinyl-*N*-alkylpyridinium), poly(4-vinylpyridine), poly(ethyleneimine), poly(vinylamine), and poly(diallyldialkylammonium). Each of them with the exception of poly(ethyleneimine) contain positively charged ions pendent to the hydrophobic polymer backbone. To date, these polyelectrolytes including anionic polyelectrolytes have been studied principally in aqueous solutions in which the hydrophobic backbones remain poorly solvated, and can promote aggregation or microphase separation because of the incompatibility of the hydrophobic backbones with water. Therefore, their various structural dynamics are related to not only the long-range electrostatic interactions but also the microphase separation that generally occurs in aqueous solutions [1–6,9,10].

In this article, we describe the interactions of a viologen polymer containing bromide as counterions with water and those in the presence of potassium and bromide ions in water by isothermal titration calorimetry (ITC). The morphology/orientation of this polymer in the solid state derived from aqueous solutions and its salt solutions is also examined by using both transmission electron microscopy (TEM) and field emission scanning electron microscopy (FESEM) techniques. The structure and designation of viologen polymer, **I**, which was used in this study, are shown below.

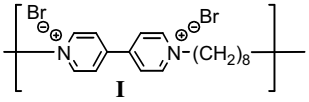

I

2. Experimental section

2.1. Materials

Polymer **I** was synthesized in our laboratory as previously reported [11,12]. In short, equimolar amounts of 4,4′-bipyridyl and 1,8-dibromooctane were reacted under stirring in *N*,*N*-dimethylformamide (DMF) at 80 °C for 72 h. A partial precipitation occurred during the polymerization reaction. At the end of polymerization reaction, the reaction flask was cooled to room temperature, and the polymer was precipitated out completely with the addition of ethyl acetate. It was filtered immediately, dried in vacuum for 24 h and stored in a desiccator [11,12]. It was characterized by FTIR, FT-NMR and elemental analysis. Anal. Calcd for $C_{18}H_{24}N_2Br_2$ (**I**): C, 50.49; H, 5.65; N, 6.54; Br, 37.32. Found: C, 51.22; H, 5.82; N, 7.06; Br, 35.75. Its measured inherent viscosity in methanol at 35 °C was 0.46 dL/g at a polymer concentration of 0.2 g/dL. It exhibited a biphasic liquid-crystalline solution at a concentration of 39 wt% and a lyotropic solution at concentration of 51 wt% in water, respectively, as determined by polarizing optical microscopy. The KBr was purchased from Sigma–Aldrich and was dried in an oven under vacuum at 80 °C overnight. All solutions were prepared using deionized water, which had a resistivity of 18 MΩ cm.

2.2. Methods

We used the following techniques to study the interactions of both polymer with water and KBr with water by microcalorimetry as well as the morphology/orientation of an ionic polymer in the solid state derived from its aqueous solutions and solutions containing specific amounts of potassium bromide salts by using TEM and FESEM.

2.3. Microcalorimetry

ITC (isothermal titration calorimetry) is a technique that measures the released or absorbed heat upon mixing of two solutions. The instrument used in this work is a VP-ITC microcalorimeter from Calorimetry Sciences Corporation (Lindon, UT). Two identical spherical cells, a reference cell and a sample cell both with a volume of 1.30 mL, are enclosed in an adiabatic jacket. The working cell is filled with the sample solution, and the reference cell is filled with the solvent water used to prepare the sample solution. The titrant is injected stepwise into working cell with a syringe of total volume of 250 μL. The sample cell is constantly stirred. For the experiments reported herein the stirring rate was 310 rpm. The measurement is performed at constant temperature of 25 °C. Small aliquots of titrant (typically 20 μL) are successively injected into the solution of working cell. The first injection is usually set to a volume of 20 μL. Because of possible dilution during the equilibration time preceding the measurement, the first injection was ignored in the analysis of the data. Each injection produces a characteristic peak in the heat flow (J/s) due to released or absorbed heat. In the analysis, a baseline is subsequently subtracted from the data. It corresponds to the signal between consecutive injections when no change in the heat flow is detected. An exothermic reaction yields a negative peak signal because of the released heat in the sample cell is no longer required from the resistive heater of the instrument. Similarly, an endothermic reaction causes a positive peak. Integrating each of the peaks provides the heat per injection. The data analysis was performed using the BindWorks software provided by Calorimetry Sciences Corporation.

2.4. TEM

The samples for transmission electron microscopy were prepared by two different methods. In the first method, droplets of a specific concentration of polymer **I** solution in water were put on 400-mesh holey carbon-coated copper grids. After 1 min of adsorption time, the excess solution was removed from the carbon film. Dried samples were studied with an energy filter transmission electron microscope (Tecnai G2 F30 S-TWIN) at an accelerating voltage 300 kV. In the second method, a thin film of polymer **I** solution of specific concentration was deposited on a 400-mesh holey carbon-coated copper grid stuck on the top of a metallic pellet on the top of a dry-ice cube. The metallic pellet holding copper grids with the frozen polymer film was then carefully removed and quickly transferred into a freeze-drying system and freeze-dried. This method retains the orientation of the polymer chains in solution before freezing, without much agglomeration in contrast to room temperature drying of polymer solutions where polymer-chain agglomeration is very significant. These samples were studied using the same TEM instrument used in the first method at an accelerating voltage of 300 kV.

2.5. FESEM

The samples for FESEM studies were prepared by depositing a thin film of a specific concentration of the polymer **I** solution on a double carbon coated tape on a metallic pellet on the top of a cube of dry-ice. The frozen polymer film with the metallic pellet was then carefully transferred into a freeze-drying system and freeze-dried. The freeze-dried sample was then gold coated and studied using JEOL JSM 6700 FESEM with an operating voltage of 8 kV. The working distance also varied from 5 to 10 mm to get the best resolution. The images were taken in both secondary electron emission mode and backscattered detection mode to get surface morphology as well as composition of the samples.

3. Results and discussion

The dilution experiments of polymer **I** solution were performed in three separate series. In the first series of runs, 104 mM polymer **I**

solution in the cell was diluted to 89.11 mM. In the second series of runs, the resultant solution of the first series of runs which was at 89.11 mM was diluted to 76.36 mM. In the third series of runs, the resultant solution of second series of runs which was at 76.36 mM was diluted to 65.43 mM. Fig. 1A shows the heat per injection obtained from integrating the heat flow curve from raw ITC data (not shown) for the three series of runs when water (20 μL/injection) was injected into polymer **I** solution (1.30 mL) in the working cell, and Fig. 1B shows the observed heat at each injection as a function of polymer **I** concentrations in the working cell. It is important to note here that in the course of a dilution measurement the polymer **I** concentration decreases in the working cell and, therefore, the slope of the heat dependent in Fig. 1B is inversed when compared with that in Fig. 1A. Similarly, dilution experiments of polymer **I** solution of concentration 12 mM were also performed under identical conditions, but their plots are not shown. However, all of these dilution experiments suggest that the dilution of polymer **I** with water is endothermic over the whole examined concentrations and the magnitude of the signal decreases with the decrease in polymer concentration. Attempts to unveil the cross-over to the exothermic signal with the further lower concentration of polymer **I** failed because of the detection limit (ca. 10 nW) of the calorimeter instrument.

Fig. 2A shows heat per injection obtained from integrating the heat flow over time (from raw ITC data, not shown) when polymer **I** solution was injected into the working cell, and Fig. 2B shows the observed heat at each injection as a function of polymer **I** concentrations in the working cell. These experiments were conducted in three parts. In the first part, 104 mM solution of polymer **I** was injected (20 injections, 20 μL/injection) into water (1.30 mL) until the polymer concentration in the cell reached 14.88 mM. In the second part, 104 mM solution of polymer **I** was injected (20 injections, 20 μL/injection) into 14.88 mM polymer solution (1.30 mL) in the cell until the polymer concentration in the cell reached 27.63 mM. In the third part, 104 mM solution of polymer **I** was injected (20 injections, 20 μL/injection) into 27.63 mM polymer

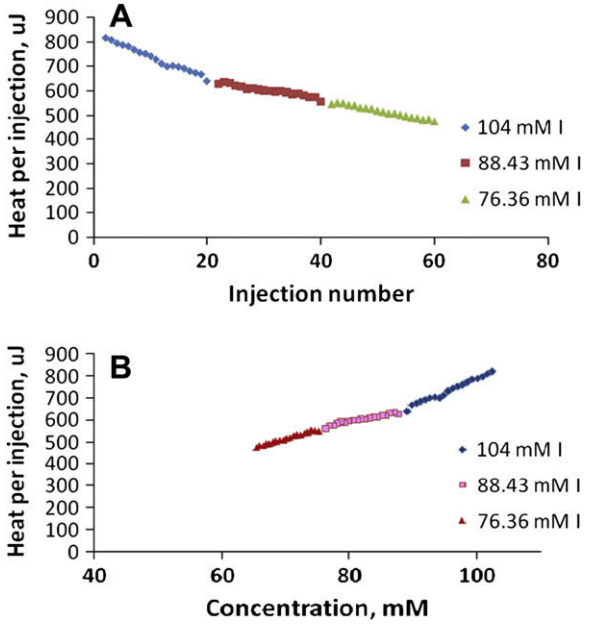

Fig. 1. (A) Heat per injection obtained from integrating the heat flow over time (from raw ITC data) when water (20 μL/injection) was injected into a 104 mM polymer **I** solution in the working cell (1.30 mL), and (B) Heat per injection as a function of polymer **I** concentrations in the working cell (1.30 mL).

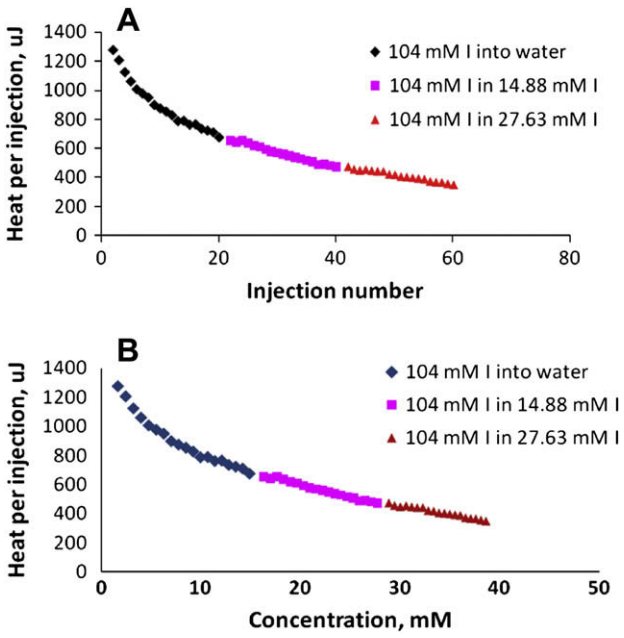

Fig. 2. (A) Heat per injection obtained from integrating the heat flow over time (from raw ITC data) when 104 mM polymer **I** solution (20 μL/injection) was injected into water in the working cell (1.30 mL), and (B) Heat per injection as a function of polymer **I** concentrations in the working cell (1.30 mL).

I solution (1.30 mL) in the cell until the polymer concentration in the cell reached 38.56 mM. Similar experiments with the concentration of 12 mM of polymer **I** were also performed under identical conditions, but their plots are not shown. All of these experiments also suggest that the interaction of polymer **I** with water is endothermic over the whole examined concentrations. But, on the

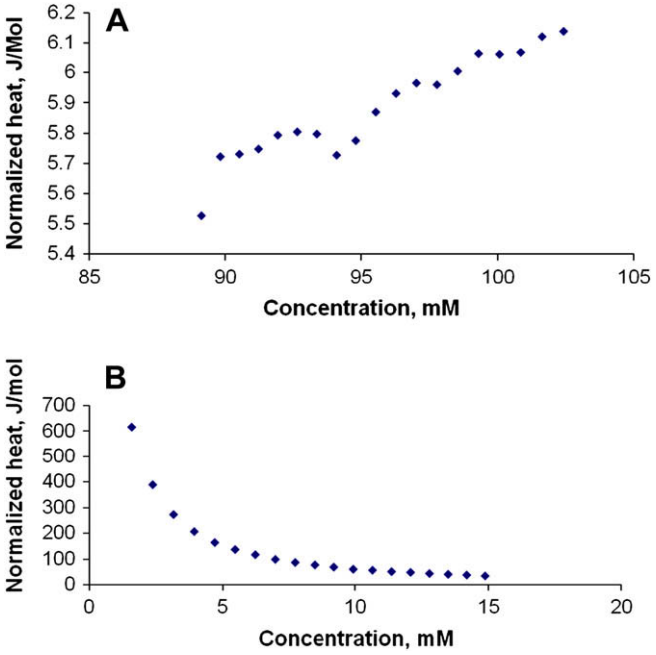

Fig. 3. (A) Normalized heat of dilutions of polymer **I** as a function of polymer concentrations when water is added to polymer solution in the working cell (1.30 mL), and (B) normalized heat of dilutions of polymer **I** as a function polymer concentrations when 104 mM polymer solution is added into water in the working cell (1.30 mL). The heat is normalized by the moles of polymer present in the system.

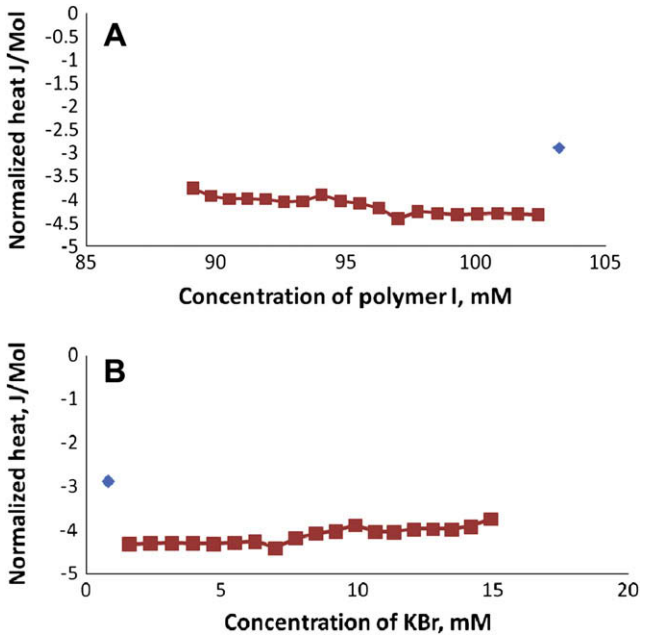

Fig. 4. (A) Normalized heat of polymer–KBr interaction (normalized by the total number of moles of polymer and KBr in the system) as a function of polymer **I** concentrations in the working cell (1.30 mL). Data points represented by ◆ represent the first injection, and (B) Normalized heat of polymer–KBr interaction (normalized by the total number of moles of polymer and KBr in the system) as a function of KBr concentrations in the working cell (1.30 mL).

contrary, the magnitude of the observed heat decreased with the increase in polymer concentration. Note here that, unlike Fig. 1A and B, in this set of experimental conditions, the slope of the heat dependent plot remained essentially identical, since the concentration of polymer increases in the working cell with the successive injections of polymer solutions. It is interesting to note that when water is added into the polymer, the process starts as endothermic and moves towards exothermic (Fig. 1A) and when the polymer is added into water the process starts at endothermic and moves towards exothermic (Fig. 2A), although our intuition suggests the opposite trend. The observed heat is endothermic in nature for the concentration range observed and decreases in magnitude with the increase in polymer concentration (Fig. 2B). This is contrary to the observation when water was added into polymer **I** solution where the magnitude of the observed heat increased with the increase in polymer concentration (Fig. 1B).

Although polyelectrolytes both rigid-rod and flexible types are becoming an interesting class of materials, their solution properties by ITC measurements are relatively rare [13]. Sinn et al. [13] reported the dilution experiments of poly(sodium acrylate), NaPAA, and poly(sodium styrenesulfonate), NaPSS, with water over a broad range of concentrations as studied by ITC and compared to the corresponding low molecular salts, sodium acetate, NaAc and sodium sulfate. Interestingly enough, NaPAA is only weakly exothermic and shows nearly ideal behavior over the whole examined range up to 1 M solutions. Its heat of dilution depends weakly on its molecular weights. In contrast, the dilution of NaAc is exothermic over the whole examined range of concentrations. The magnitude of the signal increases with concentration. The released heat suggests that there exists a local exothermic binding and rearrangement of water molecules around the acetate anion. The

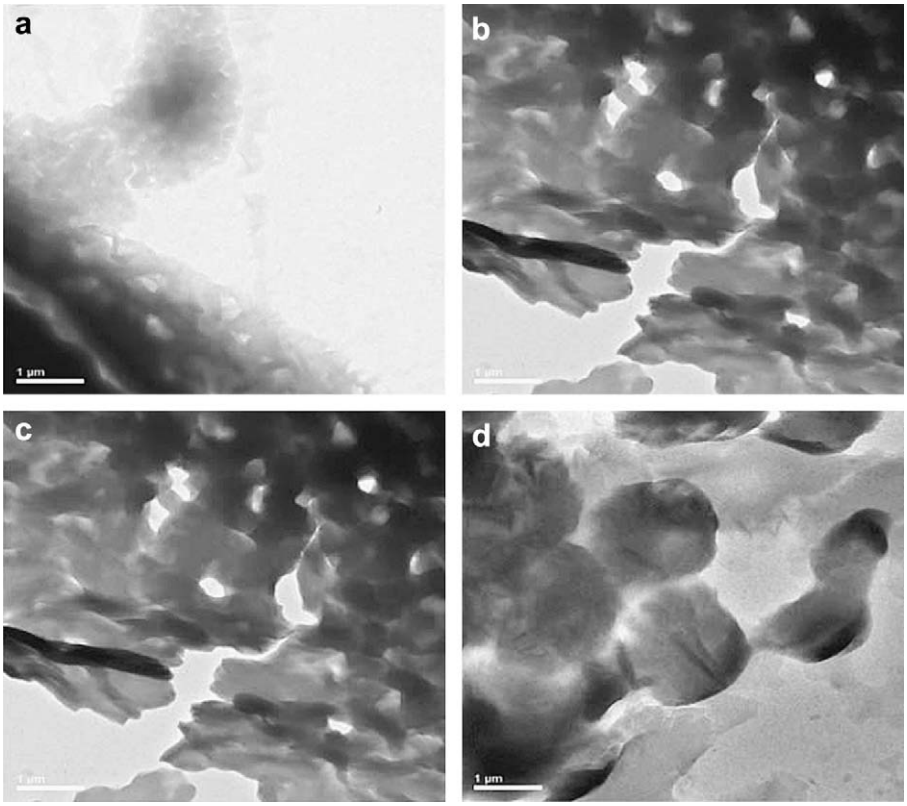

Fig. 5. TEM micrographs obtained at increasing concentrations of polymer **I** solution in water (a) 1.1, (b) 4.4, (c) 10.0, and (d) 50.0 wt% displaying gradual aggregation and overlapping aggregated structure leading to quasi-spheroidal morphology (magnification 5600×).

dilution experiments of NaPSS suggest that it is exothermic at low concentrations and turns only slightly endothermic at high concentrations. On the contrary, sodium sulfate exhibits a slight exothermic at low concentrations, but highly endothermic at high concentrations. The strikingly similar heat of dilution data of NaPAA and NaPSS obtained by ITC were quite surprising, despite they differ significantly in their chemical structures and in the polarizability of their charges. Note here that both the polymers contain the charged groups as pendent groups attached to the flexible polymer chains. However, polymer **I** is a main-chain ionic polymer having octamethylene units as hydrophobic moieties, which interacts with water apparently in a different manner leading to the endothermic process with dilution.

Fig. 3 shows the normalized heat of interaction of water with polymer **I**. At low polymer concentration, the signal is endothermic for the dilution experiment. The magnitude of the observed signal increases with increase in polymer concentration but varies only by ~0.6 J/mol (Fig. 3A) for the observed concentration range. At low concentration, when polymer was added into water, observed signal is highly endothermic and the magnitude decreased rapidly with increase in polymer concentration and attained almost steady value at high concentration. The signal remained endothermic for the observed concentration range and the magnitude of the observed signals varied by about 580 J/mol (Fig. 3B). A direct comparison of the two plots is not possible because of the different concentration range studied. However, it is clear that at higher polymer concentration the variation of the observed heat becomes very small.

Fig. 4 shows the normalized heat of interaction of salt KBr with polymer **I** as a function of both polymer and KBr concentrations. The experiment was conducted by adding 104 mM KBr solution into a solution of 104 mM polymer **I** in the working cell. Dilution heats of polymer and KBr were then substracted to get the heat of interaction of polymer with KBr. The first injection was included in the plots here in order to make the trend of the heat curve clear. It is evident from Fig. 4 that the heat of interaction of KBr with the polymer is relatively small and exothermic in nature for the observed concentration ranges of KBr and polymer. The magnitude of this heat of interaction shows a slight exothermic trend with the increase in polymer concentration (Fig. 4A) and a slight endothermic trend with the increase in KBr concentration (Fig. 4B).

Fig. 5 shows TEM micrographs of polymer **I** (prepared by first method) obtained from various concentrations from 1.1 to 50 wt% in water. It is evident from these micrographs that even at low concentration it exhibits an aggregated structure, which then develops with the further increase in polymer concentrations to quasi-spheroidal morphology. A closer look into these images reveals that with increase in polymer concentration, the polymer structure transformed into more defined morphology (which is described as quasi-spheroidal) at higher polymer concentration (cf. Fig. 5d) from random morphology at lower concentration (cf. Fig. 5a–c). This means that the samples with higher polymer concentration show more definable morphology than the other ones. To validate this observation we have now investigated the images in further details and calculated the average dimension of the quasi-spheroidal structure shown in Fig. 5d, which gives a value around 1.65 μm with roughly 10% size variation. This clearly indicates a well-defined morphology of the polymer structure with moderate size distribution. This kind of well-defined size

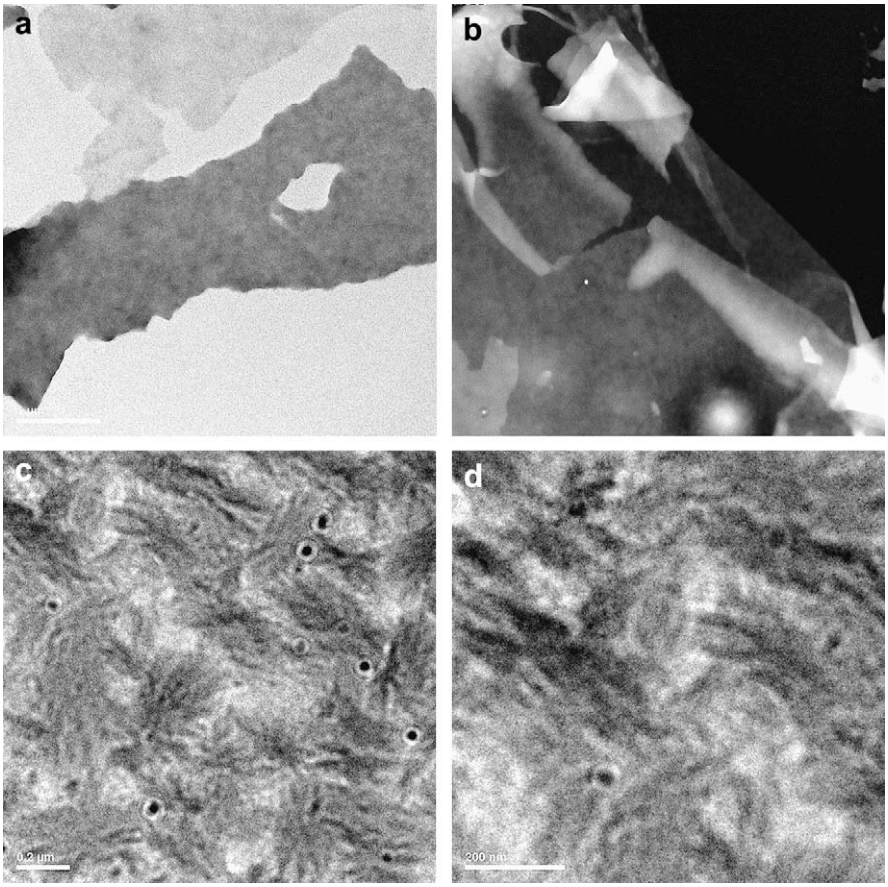

Fig. 6. (a) TEM micrograph for 12 mM polymer **I** solution in water, (b) STEM image of 12 mM polymer **I** solution, (c) TEM micrograph of 104 mM polymer solution **I** at 22,500 magnification, and (d) TEM micrograph of 104 mM polymer solution **I** at 42,000 magnification.

distribution is clearly absent for the other samples shown in Fig. 5a–c due to their random morphology. This clearly indicates that with increase in the polymer concentration the aggregated polymer takes more defined structures than random structures observed at low concentrations. This polymer also exhibited a lyotropic solution at 51 wt% in water [11]. The aggregation phenomena of ionic polymers irrespective of the nature of polyions (rigid-rod or flexible) are quite remarkable in general, since the macroions approach one another leading to the formation of aggregates instead of repulsion between like charges. The mechanism of this aggregation process remains unknown to date, but aggregation processes do occur in both flexible and rod-like polyelectrolytes as detected by various experimental techniques. For example, aggregation of flexible NaPSS in water was detected by light microscopy

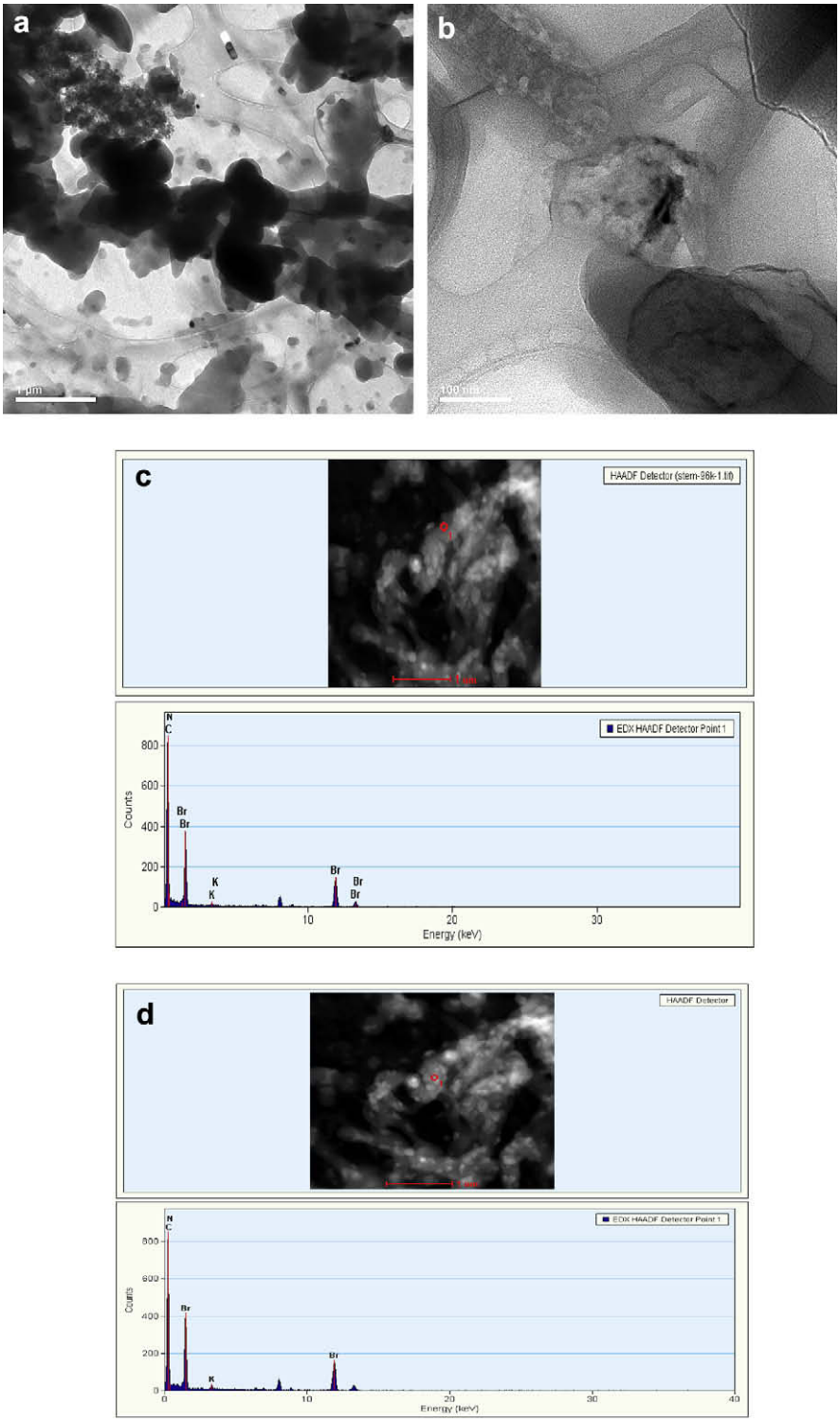

Fig. 7. TEM micrographs of mixture of KBr and polymer (a) magnification 7100×, (b) magnification 63,000×; (c) and (d) EDX image and spectra at two different spots showing the presence of salt on polymer chain.

and dynamic and static light scattering [14]. The dimensions of these aggregates increase with the increase in polymer concentration and molar mass of polymer. Similar aggregation phenomena were also detected in the rigid-rod ionic polymers of carboxylated poly(*para*-phenylene ethynylene) and sulfonated poly(*para*-phenylene) in water by dynamic and static light scattering, small-angle X-ray scattering, scanning force microcopy and TEM [15–18].

Fig. 6 shows TEM micrographs of polymer **I** prepared by the second method. At lower concentration, polymer **I** forms irregular sheet-like structures as shown in Fig. 6a and b. Fig. 6c shows irregular bundles of polymer aggregates. Each bundle consists of randomly oriented polymer chains as shown in Fig. 6d. Valleys in this Fig. 6a–d probably represent water pockets in the frozen material. It could be possible that during the freezing stage, expanding ice in those pockets forces the polymer chains to bundle and pushes those bundles out of the panes to give a rough appearance to the topology. A closer look between Figs. 5 and 6 reveals that the freeze-dried samples effectively retain the polymer chain orientation whereas the room-temperature-dried samples exhibit an aggregated structure and the degree of aggregation

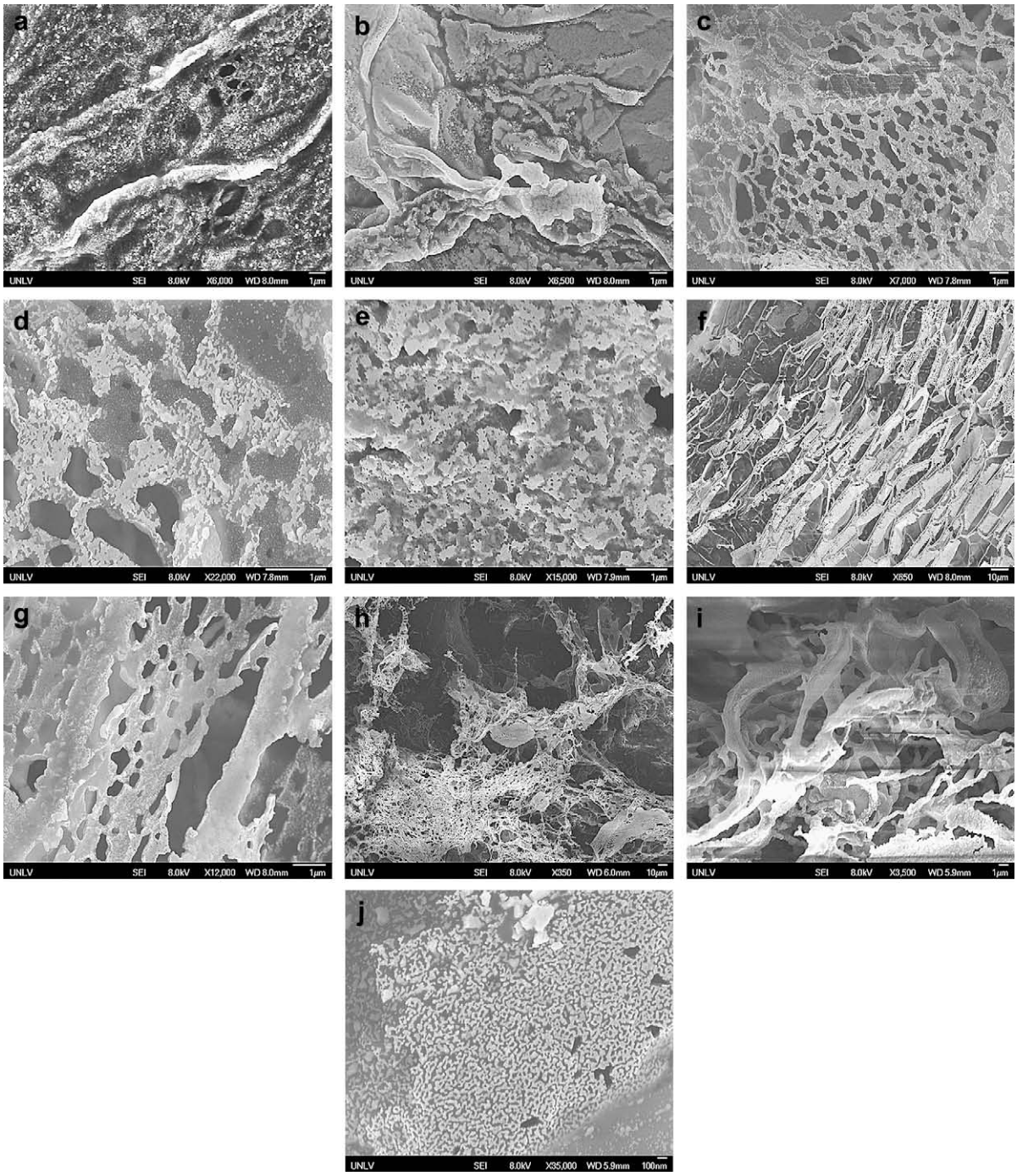

Fig. 8. FESEM micrographs obtained at different concentrations of polymer **I** solution in water (a) 1.72 mM KBr and 10.28 mM polymer, (b) 3.18 mM KBr and 8.81 mM polymer, (c) and (d) 4.44 mM KBr and 7.55 mM polymer at two different magnifications, (e) 38.56 mM KBr and 65.43 mM polymer, (f) and (g) 104 mM polymer at two different magnifications, and (h)–(j) 12 mM polymer at three different magnifications, respectively.

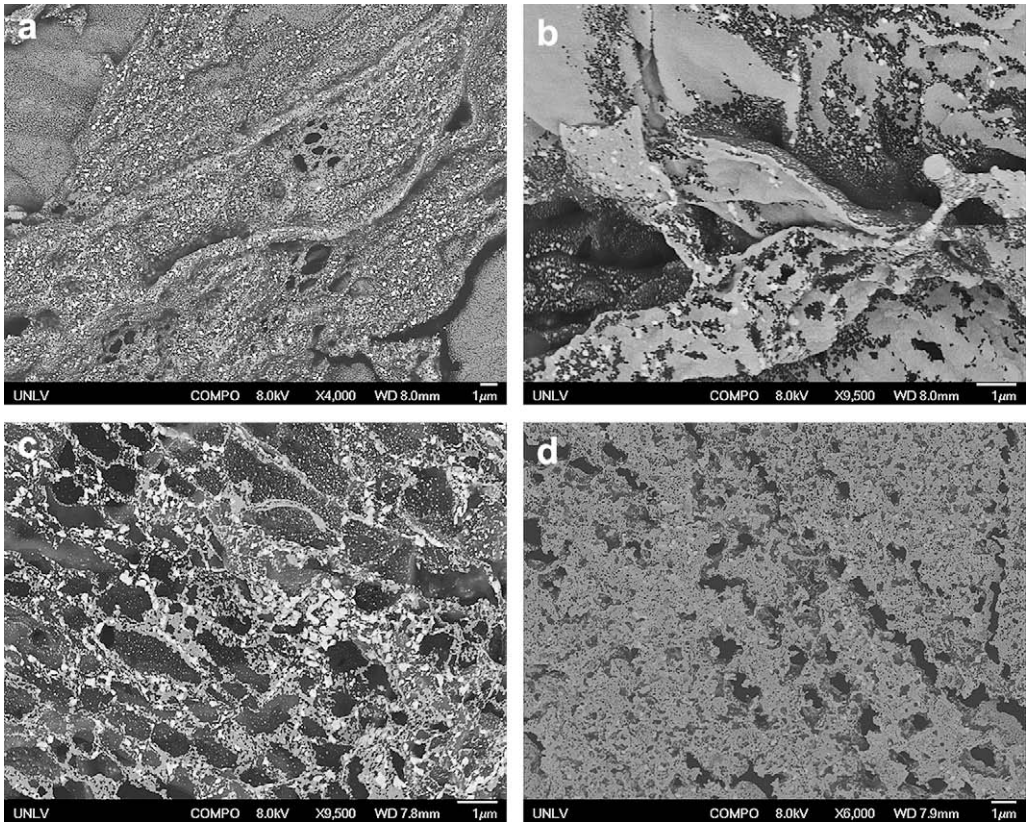

Fig. 9. Backscattered FESEM micrographs showing the salt–polymer composition of the samples at increasing salt concentrations in polymer **I** solution (a) 1.72 mM KBr and 10.28 mM polymer (S/P = 0.17), (b) 3.18 mM KBr and 8.81 mM polymer (S/P = 0.36), (c) 4.44 mM KBr and 7.55 mM polymer (S/P = 0.59), and (d) 38.56 mM KBr and 65.43 mM polymer (S/P = 0.59).

increases with the increase in the polymer concentration. This is because the excess heat energy supplied during room temperature drying leads to the re-orientation of the polymer chains and develops into the energetically favored quasi-spheroidal structure.

Fig. 7 shows TEM micrographs of a mixture of 38.5 mM KBr with 65.43 mM polymer **I**. Samples were prepared by depositing a thin film of a mixture of polymer **I** and KBr solution of the above mentioned concentration in water on a 400-mesh holey carbon-coated copper grid stuck on the top of a metal disc placed on the top of a dry-ice cube. The metal holding copper grids with the frozen sample was then carefully removed and quickly transferred into a freeze-drying system and freeze-dried. Fig. 7a and b were obtained at 7.1 and 63 K magnifications, respectively. Fig. 7a shows polymer chains with embedded salt, whereas Fig. 7b shows the orientation of the polymer coil at the time of freezing. Fig. 7c and d shows EDX images, which were measured at two different spots of the sample (shown by the red circles[1]). One is taken on a rough area of the sample (cf. Fig. 7c) and the other is taken on a smooth surface of the sample (cf. Fig. 7d) to determine the composition and distribution of the salts within the polymer chains. Existence of both K and Br is detected in the samples, as described by the EDX spectra, which reveal the presence of the corresponding salt within the samples. However, EDX spectra obtained on rough spots and smooth surface show similar composition depicting the fact that the salt is uniformly distributed within the samples.

Fig. 8a represents sample obtained by freeze-drying a solution of 1.72 mM KBr and 10.28 mM polymer (with Salt (S)/Polymer (P) = 0.17). Fig. 8a shows sponge like morphology. White specks are probably associated salt in the polymer aggregates. Fig. 8b shows sample obtained by freeze-drying a solution of 3.18 mM KBr and 8.81 mM polymer **I** solution (S/P = 0.36). It shows folded polymer sheets of corrugated morphology. Fig. 8c and d shows sample at two different magnifications obtained by freeze-drying a solution of 4.44 mM KBr and 7.55 mM polymer **I** (S/P = 0.59). These figures show polymer in lace-like morphology. Aggregates are interconnected by narrow polymer bridges. Fig. 8e shows 38.56 Mm KBr and 65.43 mM polymer **I** (S/P = 0.59). Here the aggregated polymer film appears to be thicker. A closer look at the images from Fig. 8a–e depicts that at lower concentration of the polymer **I** solution (10.28 mM or less) the orientation effect of salts on the polymer morphology is more pronounced and increases with the increase in the salt concentration. With S/P ratios increasing from 0.17 to 0.59, the polymer morphology changes from a less ordered spongy structure (cf. Fig. 8a) to an ordered interconnected bridged structure (cf. Fig. 8c and d). But at higher concentration of polymer **I** solution (65.44 mM) the orientation effect of the salt on the morphology of the polymer structure is suppressed by the presence of high percentage of polymer within the solution (cf. Fig. 8e), although the S/P ratio was maximum (0.59) in this sample with respect to the others. These results suggest that there is an optimum percentage of ions that can be introduced within the solution to get considerable orientation morphology of the polymer structure. Fig. 8f–g shows samples obtained by freeze-drying an aqueous solution of 104 mM polymer **I**. All of these figures show interconnected polymer network of lace-like morphology. Fig. 8h–j

[1] For interpretation of the references to colour in this text part, the reader is referred to the web version of this article.

shows samples obtained by freeze-drying an aqueous solution of 12 mM polymer **I**. A comparison of Fig. 8f with Fig. 8h–j shows the less ordered arrangement of the polymer aggregates with the decrease in its concentrations.

FESEM images in the backscattered detection mode are displayed in Fig. 9 for four different salt–polymer compositions. These images show the composition of the films with different concentrations of the salts within the samples. The bright specks clearly depict the presence of salts within the polymer matrix. Fig. 9a represents the sample obtained by freeze-drying an aqueous solution of 1.72 mM KBr and 10.28 mM polymer (S/P = 0.17). Fig. 9b shows sample obtained by freeze-drying an aqueous solution of 3.18 mM KBr and 8.81 mM polymer **I** solution (S/P = 0.36). Fig. 9c shows the sample obtained by freeze-drying an aqueous solution of 4.44 mM KBr and 7.55 mM polymer **I** (S/P = 0.59). As described earlier, the images clearly show the effect of the salt on the orientation morphology of the polymer matrix. With increase in the percentage of the salt with respect to the polymer, the samples become more ordered. Fig. 9d shows backscattered image of a sample obtained by freeze-drying an aqueous solution of 38.56 mM KBr and 65.43 mM polymer **I** (S/P = 0.59). Due to higher concentration of polymer **I** solution (65.44 mM) in this sample, the presence of salts is suppressed as evidenced from the image. This further suppresses the orientation effect on the polymer morphology, as clearly shown in Fig. 9 and effectively supports our previous arguments.

4. Conclusions

Dilution experiments of a main-chain viologen polymer containing bromide as counterions by ITC technique suggested that the interaction of this polymer with water is endothermic, unlike polymers NaPAA and NaPSS. This result may be related to the different mechanism of hydration of ionic groups present in the main chain of this viologen polymer. It also underwent different levels of aggregation in water producing quasi-spheroidal morphology with the increase in polymer concentrations as suggested by TEM studies. TEM studies also suggest polymer–salt association. As the polymer concentration increases the aggregated polymer takes more defined structures than random structures observed at low concentration as shown in TEM images. FESEM images show the effect of the salt on the orientation morphology of the polymer matrix. At low concentration of the polymer solution, the salt affects the ordered structure of the polymer and with an increase in the salt concentration the polymer structure becomes more ordered. The understanding of the mechanism for the formation of aggregates of ionic polymers in water as well as organic solvents is of fundamental importance to explain their supramolecular structures.

Acknowledgments

P.K.B. acknowledges the University of Nevada Las Vegas (UNLV) for New Investigation Award (NIA), Planning Initiative Award (PIA), and Applied Research Initiative (ARI) grants, and the donors of the Petroleum Research Fund, administered by the American Chemical Society, and an award (CCSA# CC5589) from Research Corporation for the support of this research. We gratefully acknowledge Markus Antonietti at the Max Planck Institute of Colloids and Interfaces for his valuable suggestions on the evaluation of ITC results and for providing us the M.S. thesis of C.G. Sinn.

References

[1] Onsager L. Ann N Y Acad Sci 1949;51:627.
[2] Noda I, Kokufuta E, editors. Polyelectrolytes. Osaka: Yamady Sci. Foundation; 1999.
[3] Holm C, Rehahn M, Oppermann W, Ballauff M. Adv Polym Sci 2004;166:1.
[4] Holm C, Joanny JF, Kremer K, Netz RR, Reineker P, Siedel C, et al. Adv Polym Sci 2004;166:67.
[5] Ise N, Sogami IS. Structure formation in solution: ionic polymers and colloidal particles. Heidelberg: Springer; 2005.
[6] Dobrynin AV, Rubinstein M. Prog Polym Sci 2005;30:1049.
[7] Thünemann AF. Prog Polym Sci 2002;27:1473.
[8] Decher G, Schlenoff JB. Multilayer thin films – sequential assembly of nanocomposite materials. Weinheim: Wiley-VCH; 2003.
[9] Förster S, Schmidt M. Adv Polym Sci 1995;120:51.
[10] Ballauff M, Blaul J, Guilleaume B, Rehahn M, Traser S, Wittemann M, et al. Macromol Symp 2004;211:1.
[11] Bhowmik PK, Han H. (Polym Prepr) Am Chem Soc Div Polym Chem 1994; 35(2):617.
[12] Bhowmik PK, Han H, Cebe JJ, Burchett RA, Sarker AM. J Polym Sci Part A Polym Chem 2002;40:659.
[13] Sinn CG, Dimova R, Antonietti M. Macromolecules 2004;37:3444.
[14] Tanahatoe JJ, Kuil ME. J Phys Chem B 1997;101:5905.
[15] Schnablegger H, Antonietti M, Göltner C, Hartmann J, Cölfen H, Samorí P, et al. J Colloid Interface Sci 1999;212:24.
[16] Wegner G. Macromol Chem Phys 2003;204:347.
[17] Kroeger A, Belack J, Larsen A, Fytas G, Wegner G. Macromolecules 2006; 39:7098.
[18] Kroeger A, Deimede V, Belack J, Lieberwirth I, Fytas G, Wegner G. Macromolecules 2007;40:105.